RSC Advances

PAPER

View Article Online
View Journal | View Issue

Cite this: *RSC Adv.*, 2014, **4**, 38804

Cobalt-based metal organic framework as precursor to achieve superior catalytic activity for aerobic epoxidation of styrene†

Guangli Yu,[a] Jian Sun,[b] Faheem Muhammad,[a] Pengyuan Wang[a] and Guangshan Zhu*[a]

Received 24th April 2014
Accepted 4th August 2014

DOI: 10.1039/c4ra03746d

www.rsc.org/advances

Novel nitrogen–cobalt catalysts have been successfully synthesized *via* one-step pyrolysis of cobalt-based metal organic framework (ZIF-67) at different temperatures under an inert atmosphere. The influence of the carbonization temperature on the porous structure of the nitrogen–cobalt catalysts is comprehensively investigated through XRD, XPS and N_2 adsorption techniques. Furthermore, the catalytic performance is investigated for epoxidation of styrene using air as the terminal oxidant. The prepared catalysts exhibit excellent styrene conversion (76.2–91.3%) with better epoxide selectivity (81.3–84.8%) in comparison with neat ZIF-67 (39.3%, 79.4%). Advantageously, the magnetically recoverable catalysts could be efficiently reused for 5 times without noticeable deterioration in activity and selectivity. This work provides an elegant approach for the development of cost-effective and practical catalysts for oxidation reactions.

Introduction

Selective oxidation of styrene to the corresponding epoxide is a pivotal industrial reaction in the production of both agrochemicals and pharmaceuticals.[1] As is well known, it is considerably difficult to activate the carbon–carbon double bonds of styrene because of its high stability. To achieve satisfactory catalytic results, conventional epoxidation processes are usually performed with homogeneous transition metal complexes (*e.g.* binaphthyl complexes, metalloporphyrins complexes, Schiff's base complexes) and hazardous oxidants (*e.g.* organic peracids, *t*-butyl hydroperoxide).[2–6] Metal complexes based on homogeneous catalytic systems inevitably lead to significant metal contamination, due to the troublesome separation process, which in turn reduces their commercial value. Alternatively, homogeneous complexes are immobilized onto an insoluble solid support to overcome this separation problem, but they still require a tedious multistep grafting procedure and the use of harsh synthetic conditions.[7,8] In addition, the phenomenon of metal leaching is likely to occur during catalytic transformation. Consequently, from environmentally friendly as well as economical viewpoint, epoxidation of styrene with eco-friendly oxidants (air/O_2) and without using any co-reductant over efficient catalysts has attracted a tremendous interest in recent years. However, the development of a cost-effective, recyclable, and easily separable heterogenized catalyst and its utilization under aerobic conditions is a challenging task from the perspective of sustainable and green chemistry.

Cobalt-based heterogeneous catalysts are widely applied in epoxidation of alkenes. Particularly, the use of O_2 without any co-reductants has aroused great interest. Tang *et al.* first reported that Co(II)-exchanged faujasite-type zeolites could catalyze styrene epoxidation using O_2 as oxidant without any other co-reductants.[9,10] Later, Co(II)-exchanged zeolite X, cobalt-substituted SSZ-51 and cobalt-substituted SBA-15 were synthesized and applied in alkene epoxidation.[11–13] Nevertheless, the above-mentioned catalytic systems have some drawbacks such as a complicated synthetic process, low epoxide selectivity and the use of pure oxygen rather than air as terminal oxidant.

Metal–organic frameworks (MOFs) have aroused a considerable attention over the past decade as they are regarded as a novel generation of ordered porous materials.[14] These intriguing materials are modularly constructed by self-assembly of linking organic ligands with metal nodes or metal clusters to form diverse network structures. Motivated by their permanent porosity, compositional and structural variability, and uniform open cavities, MOFs have emerged as ideal materials with wide-ranging applications including their use as chemical sensors, for gas adsorption, drug delivery, catalysis, and so forth.[15–20] In comparison to purely inorganic porous solids (*e.g.* zeolites or activated carbon),

[a]*Key State Key Laboratory of Inorganic Synthesis and Preparative Chemistry, College of Chemistry, Jilin University, Changchun 130012, P. R. China. E-mail: zhugs@jlu.edu.cn; Tel: +86 43185168331*

[b]*College of Chemistry, Jilin University, Changchun, 130023, P. R. China*

† Electronic supplementary information (ESI) available. See DOI: 10.1039/c4ra03746d

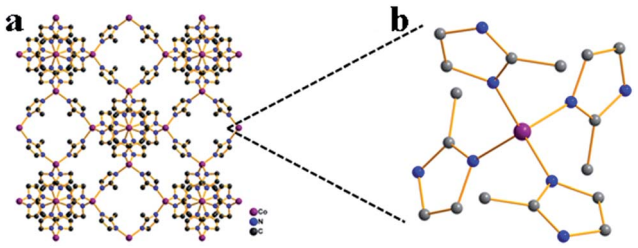

Fig. 1 (a) Structural packing of ZIF-67 along the a axis direction; (b) enlarged Co–N_4 coordinated moiety.

they present many obvious advantages, especially in the field of heterogeneous catalysis. In addition to the previously commented designed crystal engineering, the most important one is the introduction of a wealthy catalytically active transition metal-connecting points or additional functional groups into the porous MOFs structures.[21,22] In this regard, MOFs can be directly used in heterogeneous catalysis[18,23–25] or post-modified with metal complexes.[26–28] To date, only a handful of robust Co-based MOFs (such as STA-12, MFU-1, and MFU-2)[29–31] have been reported for epoxidation reactions, which achieve satisfactory catalytic results. As is well known, the relatively low chemical and thermal stability of porous MOFs prevented their development. Taken all together, the synthesis of robust metal–organic frameworks as heterogeneous catalysts with potential applications is still a challenging research goal.

In order to fabricate the required material, we reported a new experimental strategy, using porous MOF as sacrificial template to prepare catalyst for the styrene oxidation. In this approach, inexpensive cobalt imidazolate frameworks (ZIF-67), which had been used for capacitor and water treatment, are selected as premier candidates.[32,33] Structurally, as depicted in Fig. 1, each cobalt center is coordinated to four nitrogen atoms of imidazolate ligands, thus forming regularly distributed Co–N_4 moieties within the frameworks. After carbonization under an inert atmosphere, catalysts are obtained with Co–N_4 macrocycles on a carbon support, while still maintaining the porous framework. The catalysts possess uniformly distributed active sites with a high surface area. Furthermore, the presence of metallic Co^0 provided an added opportunity to magnetically separate the catalysts from the reaction mixture. As elaborated in previous work,[34] O_2 molecules can be adsorbed on the central transition metal atom (Co) of the Co–N_4 clusters. More importantly, transition metals with variable chemical valences can transfer electronic effects, which are the main active site as oxygen transfer agents. When applied as catalytic material, the porous Co–N_4 complexes provided heterogeneous catalytic sites for the selective oxidation of styrene to epoxide, even using benign air as the final oxidant. An unexpectedly high conversion (91.3%) and good epoxide selectivity (84.8%) have been obtained using ZC-700 as catalyst at an optimized temperature. Conveniently, catalysts are magnetically separated and reused 5 cycles with insignificant loss in catalytic activity and selectivity.

Experimental

Materials and methods

Cobalt nitrate hexahydrate (Co $(NO_3)_2 \cdot 6H_2O$, Sinopharm Chemical Reagent Co., Ltd., China, AR), 2-methylimidazole (MeIM, Chengdu Kelon Chemical Reagent Factory, AR), triethylamine ($C_6H_{15}N$, Tianjin Fuyu Chemical Co., Ltd., AR), styrene (Sigma-Aldrich, 98%) *N*,*N*′-dimethylformamide (DMF, Beijing Chemical Works, AR) and distilled water are used as received without any further purification.

The powder X-ray diffraction (XRD) measurements were performed on a Riguku D/MAX 2550 diffractometer using Cu-Kα radiation ($\lambda = 1.5418$ Å) and operating at 50 kV and 200 mA with a scanning step of 0.02°. X-ray photoelectron spectroscopy (XPS) was carried out on a Scienta ESCA200 spectrometer using Al-Kα radiation. For the porosity analysis, nitrogen adsorption–desorption experiments were taken at 77 K on an Autosorb iQ2 adsorptometer, Quantachrome Instrument. Prior to the tests, the samples were degassed overnight at 423 K under high vacuum. Specific surface areas were calculated by using the Brunauer–Emmett–Teller (BET) equation, and the pore size distributions were determined by applying non-local density functional theory (NL-DFT) methods. The metal content of all the catalysts was analyzed by inductively coupled plasma-atomic emission analyses (ICP-AES, Perkin-Elmer Optima 3300 DV). The magnetic properties were measured by a superconducting quantum interface device magnetometer (SQUID VSM) at room temperature.

Synthesis of ZIF-67 nanocrystals

In this work, ZIF-67 (Co-MOF) nanocrystals were prepared following a previously reported method with a slight modification.[35] Briefly, $Co(NO_3)_2 \cdot 6H_2O$ (0.717 g, 2.46 mmol) was dissolved in H_2O (50 mL); moreover, 2-methylimidazole (3.244 g, 39.5 mmol) and triethylamine (4 mL) were dispersed in another H_2O (50 mL). Afterwards, both solutions were rapidly mixed together and left stirring overnight with a magnetic bar at room temperature. Finally, the purple powders were purified by repetitive centrifugations (10 000 rpm, 2 minutes) using H_2O as the solvent with subsequent drying in air.

Preparation of heterogeneous catalysts

As-made ZIF-67 samples were placed inside a quartz boat, which was introduced in the middle of a quartz tube with both ends connected to argon gas. The tubular furnace was heated up at different temperatures from 600 to 900 °C for 5 hours under a continuous argon flow of 50 mL min^{-1} with a heating ramp of 1° min^{-1}. After natural cooling to room temperature, the resultant catalysts were obtained and designed as ZC-*T*, where *T* referred to carbonization temperature (600, 700, 800 and 900 °C).

Catalytic epoxidation of styrene

Styrene epoxidation with air was performed in a two-necked flask (50 mL) equipped with a liquid condenser and air pump.

In a typical procedure, styrene (2 mmol) was used as substrate and the nanocatalysts (50 mg) were added into DMF solution (8 mL). Then, the mixture was refluxed at the optimized temperature for 6 h, and air was introduced at a stable flowing rate of 80 mL min^{-1}. After completion of the reaction, the nanocatalysts were recovered using a magnet, washed with acetonitrile and ethanol, dried at vacuum and reused without further purification. The products of epoxidation reaction were quantified and monitored *via* gas chromatography (Shimadzu, GC-8A) equipped with a HP-5 capillary column and a FID detector. The reaction kinetics was monitored *via* withdrawing 0.1 μl of the reaction liquid at 0.5 h intervals and analysing the measurements by GC. Calibration of GC peak areas of styrene and epoxide was performed through solutions with known amounts of styrene and epoxide in DMF. The conversion was calculated on the basis of the molar percent of styrene. The initial molar percent of styrene was divided by the initial area percent to obtain the response factor. The unreacted moles of styrene remaining in the reaction mixture were calculated by multiplying the response factor by the area percentage of the GC peak for styrene obtained after the reaction.[11] In most of the reaction conditions, styrene polymerization was negligible; thus, the polymers in the reaction products were not considered.[36] The conversion of styrene, selectivity and the yield of the products were calculated using the formulae:

$$\text{Styrene conversion (\%)} = (\text{(initial mol\%)-(final mol\%)})/\text{(initial mol\%)} \times 100$$

$$\text{The product selectivity (\%)} = \text{GC peak area of the product/GC peak area of all products} \times 100$$

$$\text{The product yield (\%)} = \text{Styrene conversion (\%)} \times \text{the product selectivity (\%)}$$

Results and discussion

XRD measurements

The crystalline structures of as-prepared ZIF-67 and their corresponding C–N–Co nanocomposite materials (labeled as ZC-600, ZC-700, ZC-800, and ZC-900) with varying carbonization temperatures are analyzed by powder X-ray diffraction (XRD), where the number (600, 700, 800 or 900) refers to the carbonization temperature. As shown in Fig. 2a, the XRD diffractogram of as-prepared Co-MOF displays high phase purity, which agrees with the well-known simulated ZIF-67 crystal structure. Fig. 2b shows that all the samples undergo structural transformation after annealing, and they no longer preserve a long-range ordered structure. Moreover, they exhibit similar patterns except for the increasing intensity of the XRD peaks. It can be clearly seen that characteristic carbon (002) broadened peaks at around 25° (2θ) represent the carbonaceous material formation upon thermal activation of the ZIF-67 precursor. The other peaks at 44.2°, 51.5° and 75.9° can be well ascribed to (111), (200) and (220) lattice facets of the β-Co, respectively, associated with standard JCPDS card no. 43-1003. Moreover, the carbonization temperature has a strong effect on the degree of the metallic Co. We can state that, with increasing annealing temperature, the diffraction peaks become stronger and sharper. These results presumably indicate that most of the Co^{2+} ions break away from the ZIF-67 frameworks, and then the resulting nanoparticles undergo further coalescence to form larger metallic Co particles.[37]

Adsorption measurements

The textural properties of parent ZIF-67 and C–N–Co catalysts are determined by N_2 adsorption–desorption isotherms at 77 K (Fig. 3) and the related parameters are listed in Table S1.† Obviously, the curve of ZIF-67 is a typical type-I isotherm, indicating that the ZIF-67 precursor has mainly microporous characteristics. After the carbonization reaction, ZC-600, ZC-700, ZC-800 and ZC-900 exhibit N_2 isotherms close to type-IV with small hysteresis loops, which suggest the presence of mesopores in the obtained carbon framework. The value of S_{BET} decreases from 282 to 94 m^2g^{-1} with thermal treatment temperature increasing from 600 °C to 900 °C (Table S1†), originating from the emission of carbon from specific edge areas at elevated temperature. As has been previously reported,[37–39] metallic cobalt still remains in the carbon skeleton, which indirectly reduces BET values. The pore size distribution (PSD) curves give plenty of information regarding the assignment of different pore sizes (Fig. 3b). As expected, the pore size

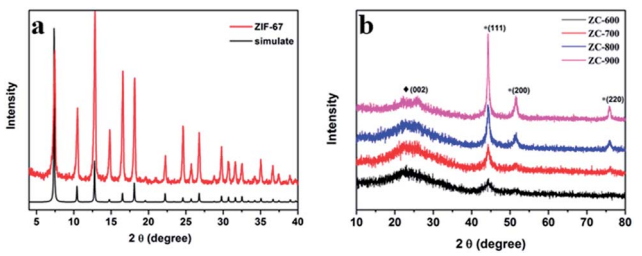

Fig. 2 XRD patterns of (a) as-prepared ZIF-67 and (b) the corresponding C–N–Co hybrid materials at different carbonization temperatures: carbon (◆) and metallic Co (*).

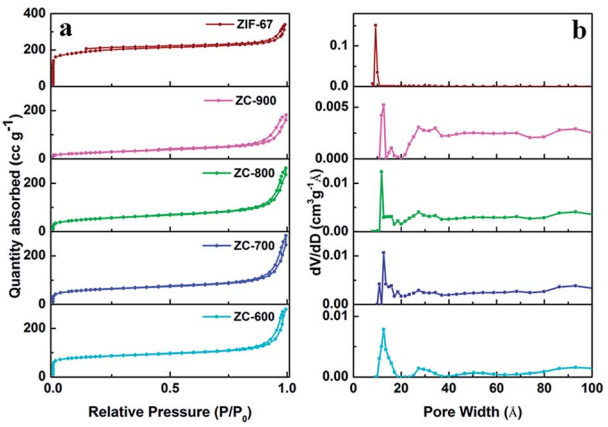

Fig. 3 (a) Nitrogen adsorption–desorption isotherms and (b) corresponding NL-DFT pore size distributions of ZIF-67, ZC-600, ZC-700, ZC-800 and ZC-900 catalysts.

of freshly prepared ZIF-67 precursor is distributed merely in the micropore region (8 to 11 Å), of which one outstanding point is the emergence of the bimodal pore distribution after the samples are heat-activated at different temperatures. Similar to ZIF-67 precursor, a noteworthy fraction of micropores (10–16 Å) in C–N–Co catalysts is formed, and mesopores mainly ranging from 20 to 40 Å are also observed. This bimodal distribution may arise from the breakdown of ZIF-67 precursor to form a carbonaceous structure.

Magnetism measurements

The magnetic properties of the nanocomposite materials (C–N–Co) are studied at room temperature with a vibrating sample magnetometer (VSM) (Fig. 4). The synthesized C–N–Co nanoparticles display a representative hysteresis loop, indicating the presence of ferromagnetism features (Fig. 4a). The magnetization saturation (Ms) values of ZC-600, ZC-700, ZC-800 and ZC-900 were found to be 49.6, 59.1, 74.1 and 93.4 emu g^{-1}, respectively. These differences are possibly caused by the crystallinity of the magnetic Co^0 particles under different carbonization temperatures, which also has been corroborated by XRD analysis. More importantly, the dispersed aqueous solution of ZC-700 material can be quickly attracted towards a regular magnet (<15 s), leaving the solution transparent and clear (inset of Fig. 4b). After the removal of the outside magnetic field, the ZC-700 material can be quickly redispersed by slight shaking, illustrating a strong susceptibility for efficient redispersibility and magnetic responsiveness.

XPS measurements

To better understand the active sites of a catalyst, it is of great importance to investigate the nitrogenous species on the carbon surface before and after the heat-treatment ZIF-67 precursor *via* X-ray photoelectron spectroscopy (XPS) (Fig. 5). The images of the full spectrum of the samples are represented in Fig. 5a. The percentage of nitrogen for ZIF-67, ZC-600, ZC-700, ZC-800, and ZC-900 is calculated from survey spectra to be around 15.07%, 8.22%, 5.09%, 2.53% and 1.65%, respectively. It is reasonably surmised that more N atoms will overflow along with the increase of the pyrolysis temperature. In Fig. 5b–f, the N1s region spectra are deconvoluted into three components: N1 (pyridinic-N), N2 (Co–N_x) and N3 (graphitic-N). The three components are shown schematically in Fig. S1† and the distributions of the three species of nitrogen atoms are particularly compiled in Table 1. Remarkably, the intensity of these three peaks significantly depends on the evolution of the annealing temperature. From Fig. 5b, for starting material ZIF-67, the existence of an only peak at N2 (BE 399.1 eV) that corresponds to N of 2-methylimidazole ligand thoroughly coordinated to Co. After annealing, the other two peaks of N1

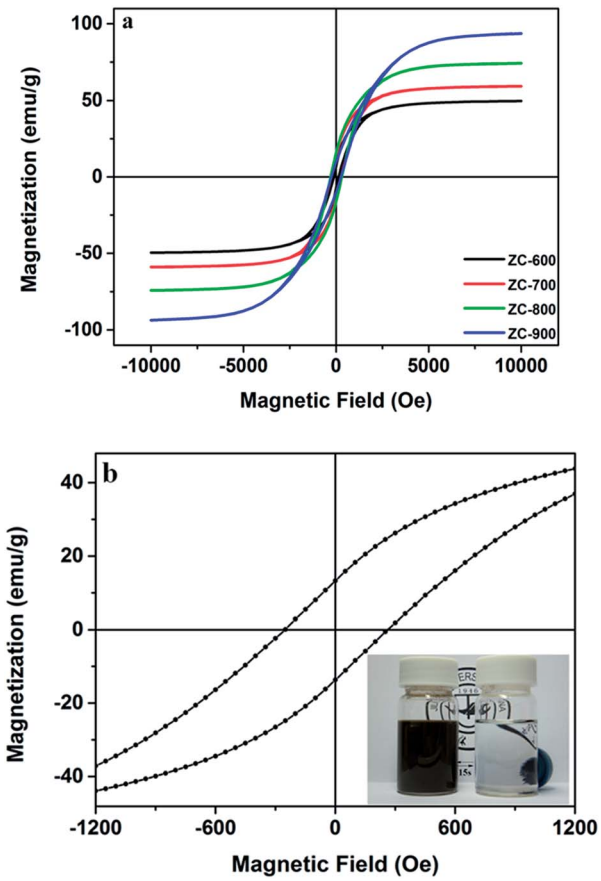

Fig. 4 (a) M–H curves of the C–N–Co composites formed by annealing at different temperatures (600 °C, 700 °C, 800 °C, and 900 °C) and (b) an enlarged curve for ZC-700 catalyst.

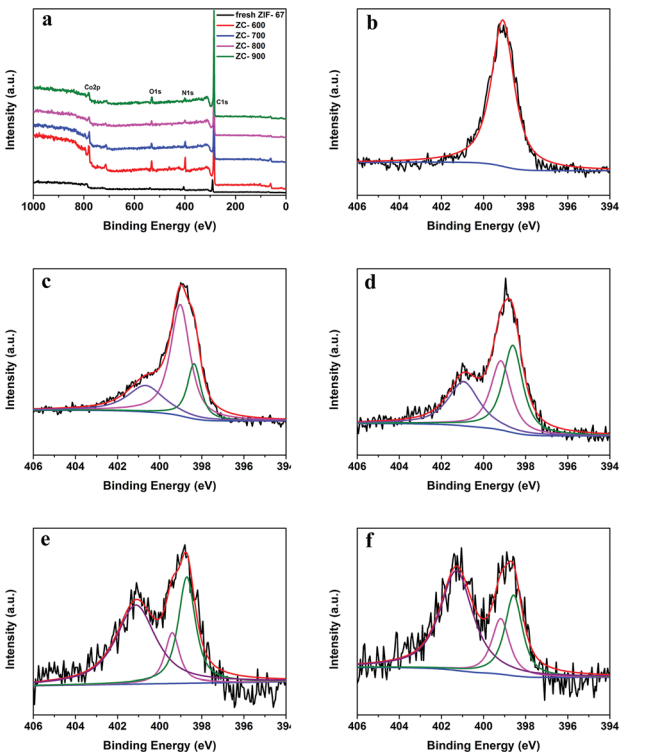

Fig. 5 (a) XPS survey spectra of fresh ZIF-67 and C–N–Co composites. (b–f) High-resolution XPS spectra of the deconvoluted N1s peak: (b) ZIF-67, (c) ZC-600, (d) ZC-700, (e) ZC-800, and (f) ZC-900.

Table 1 Ratio analysis of C, O, Co and heterocyclic N components of all as-prepared samples from XPS analysis

				N (%)			
Sample	C (%)	O (%)	Co (%)	Total	N1	N2	N3
ZC-600	86.3	3.48	1.93	8.22	19	56	25
ZC-700	90.5	2.5	1.8	5.09	38	31	30
ZC-800	94.15	2.12	1.21	2.53	32	13	55
ZC-900	91.46	5.31	1.58	1.65	25	17	58
ZIF-67	74.92	5.29	4.72	15.07	—	100	—

(BE 398.5 eV) and N3 (BE 401.1 eV) appear, whereas N2 peak becomes weaker due to 2-methylimidazole ligands ring opening, as shown in Fig. 5c–f. Upon further increasing of the pyrolysis temperature for ZC-800 and 900 (Fig. 5e and f), the percentage composition of the N2 and N1 peak becomes much lower, whereas the peaks of N3 rise dramatically. This confirms that the formed N3 is much more stable than N1 at high temperatures, in agreement with previous reports.[40] Among them, ZC-700 presents the highest assignment of N1, accompanied with a high quantity of N2 (Table 1). Based on this analysis, appropriately arranged N1 (pyridinic N) moieties with electron-donating properties are able to trap plentiful transitional metals to serve as outstanding metal-coordination ($Co–N_X$) active sites.[41] Furthermore, free N1 atoms have excellent electronic storage ability to activate molecular oxygen under mild conditions. ZC-700 probably has a better catalytic activity, and thus it will be further discussed later.

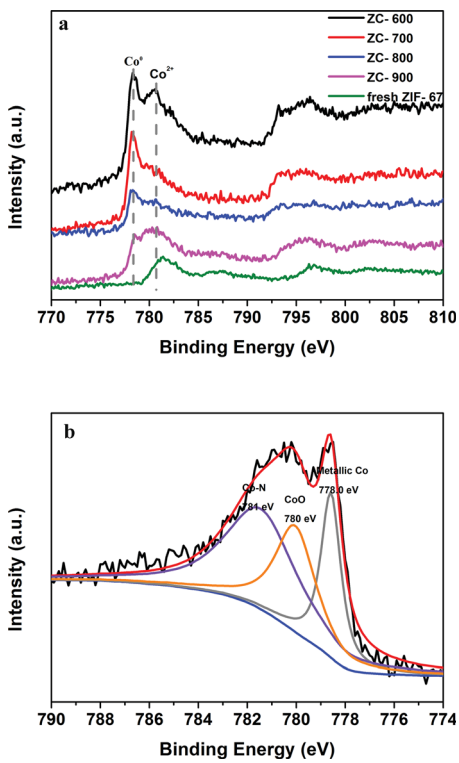

Fig. 6 (a) XPS Co2p spectra of the studied samples and (b) XPS Co2p spectra of ZC-700 catalyst.

The Co2p XPS spectra of all samples are also shown in Fig. 6. As depicted in Fig. 6a, metallic Co^0 (BE 778 eV) can be detected from ZC-600, ZC-700, ZC-800 and ZC-900, respectively, compared to ZIF-67 precursor, which is in accordance with XRD and magnetism results. After deconvolution of the Co2p (Fig. 6b), a dominant peak of ZC-700 catalyst is seen at ~781.2 e V, which is ascribed to N-coordinated metal ($Co–N_X$),[42,43] which serves as an effective activity center. Undoubtedly, the formation of Co–N bonds in nitrogen–cobalt macrocyclic catalyst shows promising applications in the selective epoxidation of styrene (see below).

Catalytic properties

As-synthesized catalysts with varying carbonization temperature have been utilized for the selective epoxidation of styrene using low-cost air as only oxidant to evaluate the catalytic performance and to understand the temperature selective catalytic activity. Table 2 lists the epoxidation of styrene over various cobalt-based catalysts. For the pure ZIF-67, 79.4% of epoxide selectivity is acquired when air is used, but the styrene conversion (39.3%) is extremely low, presumably due to the poor electron storage or the transfer nature of the organic framework. To our delight, the catalytic activity is obviously improved when ZIF-67 precursor is heat-activated under argon atmosphere at different temperatures, as is shown in Table 2. In detail, the conversion efficiency of styrene is enhanced from low (76.2% for ZC-600, entry 2) to maximum (91.3% for ZC-700, entry 3) before returning to low (77.1% for ZC-900, entry 5) again. These promising results strongly demonstrate the dependence of the catalytic reaction on the annealing temperature. Moreover, different catalytic sites also affect the epoxidation of styrene activity. It is intriguing to note that the ZC-700 catalyst exhibits an especially high activity in terms of both high conversion (91.3%) and good epoxide selectivity (84.8%). The excellent catalytic results of ZC-700 sample maybe ascribed to the following reasons. The higher content of N1 and N2 in ZC-700 catalyst (Table 1) than other C–N–Co catalysts might be responsible for the higher catalytic performance, since its catalytic active center ($Co–N_4$ structure) promotes the activation of O_2 molecules. Accordingly, ZC-800 and ZC-900, have low contents of nitrogen, and therefore, they show less activity. Furthermore, some reports[44,45] have explained this activity by stating that the nitrogen atoms containing units could pointedly enhance the electron-donor capability *via* conjugated π-system of the carbon matrix, resulting in a promotion of the interaction between catalysts and reactants. Lastly, the $Co–N_X$ moieties are stabilized only under lower temperatures.[41,46] Such issues indicate that ZC-700 catalyst possesses the highest catalytic properties. Further studies were thus performed using ZC-700 as an oxidation catalyst. In addition, DMF plays an important role in the aerobic epoxidation of styrene, and the coordination of DMF with cobalt(II) sites can promote the activation of O_2 molecules to form an active intermediate, which further interacts with styrene to produce epoxide.

Table 2 Various catalysts in epoxidation of styrene with air[a]

			Product selectivity (%)		Product yield (%)	
Entry	Catalyst	Con. (%)	Epoxide	Benzaldehyde	Epoxide	Benzaldehyde
1	ZIF-67	39.3	79.4	20.6	31.2	8.1
2	ZC-600	76.2	81.3	18.7	61.9	14.3
3	ZC-700	91.3	84.8	15.2	77.4	13.9
4	ZC-800	84.2	83.5	16.5	70.3	13.9.
5	ZC-900	77.1	82.6	17.4	63.7	13.4
6[b]	ZC-700	27.1	76.3	23.7	20.7	6.4
7[c]	ZC-700	41.9	75.4	24.6	31.6	10.3
8[d]	ZC-700	92.5	79.8	20.2	73.8	18.7

[a] Reaction conditions: styrene (2 mmol), DMF (8 mL), catalyst (50 mg), flow rate of air (80 mL min^{-1}), reaction time (5 h), reaction temperature (100 °C). [b] The reaction was performed at 80 °C. [c] The reaction was performed at 90 °C. [d] The reaction was performed at 110 °C.

The temperature dependence study of the epoxidation reaction was also carried out (Table 2, entries 6–8). It is obvious that the styrene conversion and epoxide selectivity sharply increase along with the reaction temperature from 80 to 100 °C, while the epoxide selectivity starts to somewhat decrease at higher temperatures (110 °C). This result demonstrates that the reaction temperature has a great influence on the catalytic performance. High temperature (100 °C) contributes to the progress of the reaction, but further elevating temperature readily triggers deep oxidation, and accordingly leads to lower epoxide selectivity. In the course of this study, 100 °C is found to be an appropriate reaction temperature for maximum activity.

The catalytic performance of ZC-700 catalyst for aerobic epoxidation of styrene was compared with earlier reported Co-containing heterogeneous catalysts (Table 3). It is obvious that ZC-700 catalyst gives the highest styrene conversion (91.3%) and good epoxide selectivity (84.8%) without any initiator. From entry 5 to 8, Co-containing heterogeneous catalysts show relatively poor styrene conversion and low epoxide selectivity. From entry 2 to 4, though Co-containing heterogeneous catalysts achieve satisfactory styrene conversion and epoxide selectivity, they have to use hazardous and expensive initiators (TBHP or isobutyraldehyde), which is a problem from the economic and environmental point of view. These results corroborate that ZC-700 catalyst acts as an efficient catalyst in aerobic epoxidation of styrene with air as an oxidant.

In order to further elucidate its catalytic activity, recycling tests of ZC-700 catalyst were conducted and the obtained results are shown in Fig. 7. After each reaction, the catalyst was conveniently separated with a magnet, washed thoroughly with ethanol, dried under vacuum and reused for the subsequent cycles. It was confirmed that the styrene conversion and the selectivity remained more or less the same, even after using it for 5 consecutive cycles, suggesting an outstanding stability and recyclability. Moreover, a leaching experiment was performed to verify the heterogeneity of the catalytic process. Initially, styrene (2 mmol) and the ZC-700 (50 mg) were added into a DMF solution (8 mL). The mixture was refluxed at 100 °C and air was introduced with at a stable rate of 80 mL min^{-1}. After 2 h, the ZC-700 catalyst was removed by magnet separation under a hot

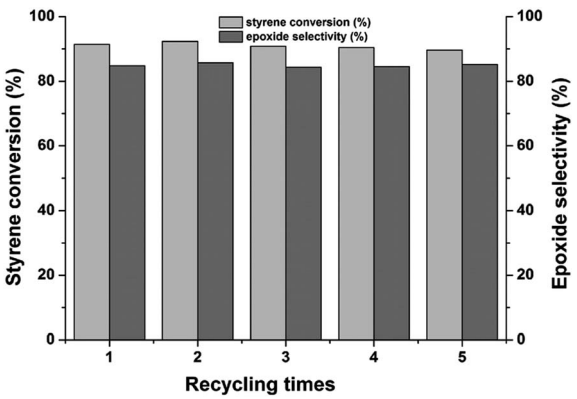

Fig. 7 Recycling experiments of ZC-700 catalyst for the epoxidation of styrene with air.

Table 3 Comparison of ZC-700 with earlier reported Co-containing heterogeneous catalysts for aerobic epoxidation of styrene

Entry	Catalyst	Oxidant	Con. (%)	Epoxide selectivity (%)	References
1	ZC-700	air	91.3	84.8	This work
2	Fe_3O_4@SiO_2–Co	air + isobutyraldehyde	90.8	63.7	47
3	Co_3O_4	air + TBHP	81.8	84.1	48
4	Co-5a	air + TBHP	89.4	90.2	49
5	Co-SSZ-S-10	O_2	24	62	13
6	Co^{2+}-X	O_2	44.2	60	10
7	Co^{2+}-NaX	O_2	44	60	9
8	Co^{2+}-MCM-41	O_2	45	62	9

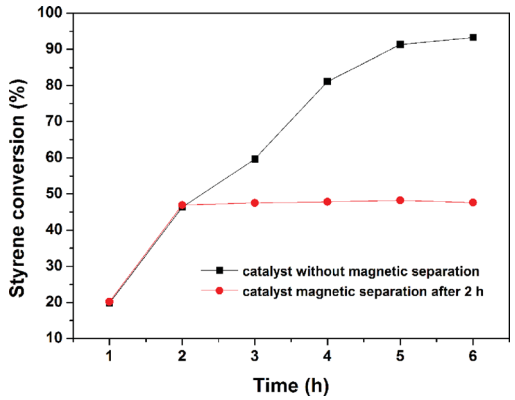

Fig. 8 (a) Kinetic profile of aerobic epoxidation of styrene and (b) leaching experiment of ZC-700 (continuing the reaction after the catalysts removing after 2 h).

solution, and the reaction proceeded for another 4 h (Fig. 8). No visible improvement in styrene conversion was observed. In addition, the result of ICP-AES analysis revealed that the concentration of Co(II) ions in the supernatant corresponds to negligible catalyst leaching (0.32 ppm). These results indicate that ZC-700 catalyst is rather stable in the catalytic process.

Conclusions

In summary, in this contribution, we successfully established a simple and efficient strategy for the fabrication of well-structured nitrogen–cobalt catalysts with a significantly and uniformly distributed catalytic center. Appropriate calcination temperature has been demonstrated to be the principal factor for achieving nitrogen–cobalt macrocyclic catalysts with high selectivity and conversion. ZC-700 catalyst exhibits extraordinary good properties in styrene epoxidation under relatively mild conditions thanks to the effective active sites. Moreover, air as a final oxidant is suitable and offers practical benefits for this process. It highlights that the ferromagnetic characteristics of nitrogen–cobalt catalysts can be used for magnetic separation of catalysts, and they can be reused 5 times with little or no loss in catalytic activity and epoxide selectivity. These results undoubtedly prove that MOFs-templated synthetic strategy could be facilely extended to the preparation of other porous catalysts with well-defined structures and high-performance. This process is easily scalable for the catalyst industry.

Acknowledgements

We are grateful to the financial supports from National Basic Research Program of China (973 Program, grant no.2012CB821700), and NSFC project (grant no. 21120102034, 20831002).

Notes and references

1 Q.-H. Xia, H.-Q. Ge, C.-P. Ye, Z.-M. Liu and K.-X. Su, *Chem. Rev.*, 2005, **105**, 1603–1662.
2 K. C. Gupta and A. K. Sutar, *Coord. Chem. Rev.*, 2008, **252**, 1420–1450.
3 E. Rose, B. Andrioletti, S. Zrig and M. Quelquejeu-Etheve, *Chem. Soc. Rev.*, 2005, **34**, 573–583.
4 R. A. Sheldon, *Homogeneous and heterogeneous catalytic oxidations with peroxide reagents*, Springer, 1993, vol. 164. pp. 21–43.
5 I. V. Khavrutskii, D. G. Musaev and K. Morokuma, *Proc. Natl. Acad. Sci. U. S. A.*, 2004, **101**, 5743–5748.
6 S. Bhor, M. K. Tse, M. Klawonn, C. Döbler, W. Mägerlein and M. Beller, *Adv. Synth. Catal.*, 2004, **346**, 263–267.
7 J. Sun, Q. Kan, Z. Li, G. Yu, H. Liu, X. Yang, Q. Huo and J. Guan, *RSC Adv.*, 2014, **4**, 2310–2317.
8 L. Ma, F. Su, X. Zhang, D. Song, Y. Guo and J. Hu, *Microporous Mesoporous Mater.*, 2014, **184**, 37–46.
9 Q. Tang, Q. Zhang, H. Wu and Y. Wang, *J. Catal.*, 2005, **230**, 384–397.
10 Q. Tang, Y. Wang, J. Liang, P. Wang, Q. Zhang and H. Wan, *Chem. Commun.*, 2004, 440–441.
11 J. Sebastian, K. M. Jinka and R. V. Jasra, *J. Catal.*, 2006, **244**, 208–218.
12 H. Cui, Y. Zhang, L. Zhao and Y. Zhu, *Catal. Commun.*, 2011, **12**, 417–420.
13 K. M. Jinka, S. M. Pai, B. L. Newalkar, N. V. Choudary and R. V. Jasra, *Catal. Commun.*, 2010, **11**, 638–642.
14 G. Ferey, *Chem. Soc. Rev.*, 2008, **37**, 191–214.
15 S. Achmann, G. Hagen, J. Kita, I. M. Malkowsky, C. Kiener and R. Moos, *Sensors*, 2009, **9**, 1574–1589.
16 N. L. Rosi, J. Eckert, M. Eddaoudi, D. T. Vodak, J. Kim, M. O'Keeffe and O. M. Yaghi, *Science*, 2003, **300**, 1127–1129.
17 M. Latroche, S. Surble, C. Serre, C. Mellot-Draznieks, P. L. Llewellyn, J. H. Lee, J.-S. Chang, S. H. Jhung and G. Ferey, *Angew. Chem., Int. Ed.*, 2006, **45**, 8227–8231.
18 A. C. McKinlay, R. E. Morris, P. Horcajada, G. Ferey, R. Gref, P. Couvreur and C. Serre, *Angew. Chem., Int. Ed.*, 2010, **49**, 6260–6266.
19 J. Lee, O. K. Farha, J. Roberts, K. A. Scheidt, S. T. Nguyen and J. T. Hupp, *Chem. Soc. Rev.*, 2009, **38**, 1450–1459.
20 F. Llabresixamena, O. Casanova, R. Galiassotailleur, H. Garcia and A. Corma, *J. Catal.*, 2008, **255**, 220–227.
21 P. Horcajada, S. Surble, C. Serre, D.-Y. Hong, Y.-K. Seo, J.-S. Chang, J.-M. Greneche, I. Margiolaki and G. Ferey, *Chem. Commun.*, 2007, 2820–2822.
22 C.-D. Wu, A. Hu, L. Zhang and W. Lin, *J. Am. Chem. Soc.*, 2005, **127**, 8940–8941.
23 A. Dhakshinamoorthy, M. Alvaro and H. Garcia, *Catal. Sci. Technol.*, 2011, **1**, 856–867.
24 A. Dhakshinamoorthy, M. Opanasenko, J. Čejka and H. Garcia, *Catal. Sci. Technol.*, 2013, **3**, 2509–2540.
25 J. Zhang, A. V. Biradar, S. Pramanik, T. J. Emge, T. Asefa and J. Li, *Chem. Commun.*, 2012, **48**, 6541–6543.
26 M. A. Gotthardt, A. Beilmann, R. Schoch, J. Engelke and W. Kleist, *RSC Adv.*, 2013, **3**, 10676–10679.
27 C. M. Granadeiro, A. D. S. Barbosa, P. Silva, F. A. A. Paz, V. K. Saini, J. Pires, B. de Castro, S. S. Balula and L. Cunha-Silva, *Appl. Catal., A*, 2013, **453**, 316–326.

28 Z. Sun, G. Li, H.-o. Liu and L. Liu, *Appl. Catal., A*, 2013, **466**, 98–104.
29 M. J. Beier, W. Kleist, M. T. Wharmby, R. Kissner, B. Kimmerle, P. A. Wright, J. Grunwaldt and A. Baiker, *Chem.–Eur. J.*, 2012, **18**, 887–898.
30 M. Tonigold, Y. Lu, B. Bredenkötter, B. Rieger, S. Bahnmüller, J. Hitzbleck, G. Langstein and D. Vollkmer, *Angew. Chem., Int. Ed.*, 2009, **48**, 7546–7550.
31 M. Tonigold, Y. Lu, A. Mavrandonakis, A. Puls, R. Staudt, J. Möllmer, J. Sauer and D. Volkmer, *Chem.–Eur. J.*, 2011, **17**, 8671–8695.
32 N. L. Torad, R. R. Salunkhe, Y. Li, H. Hamoudi, M. Imura, Y. Sakka, C. Hu and Y. Yamauchi, *Chem.–Eur. J.*, 2014, **20**, 7895–7900.
33 N. L. Torad, M. Hu, S. Ishihara, H. Sukegawa, A. A. Belik, M. Imura, K. Ariga, Y. Sakka and Y. Yamauchi, *small*, 2014, **10**, 2096–2107.
34 G. F. Wang, N. Ramesh, A. Hsu, D. Chu and R. R. Chen, *Mol. Simul.*, 2008, **34**, 1051–1056.
35 R. Banerjee, A. Phan, B. Wang, C. Knobler, H. Furukawa, M. O'Keeffe and O. M. Yaghi, *Science*, 2008, **319**, 939–943.
36 H. Cui, Y. Zhang, Z. Qiu, L. Zhao and Y. Zhu, *Appl. Catal., B*, 2010, **101**, 45–53.
37 S. Ma, G. A. Goenaga, A. V. Call and D.-J. Liu, *Chem.–Eur. J.*, 2011, **17**, 2063–2067.
38 W. Xia, J. Zhu, W. Guo, L. An, D. Xia and R. Zou, *J. Mater. Chem. A*, 2014, **2**, 11606–11613.
39 X. Wang, J. Zhou, H. Fu, W. Li, X. Fan, G. Xin, J. Zheng and X. Li, *J. Mater. Chem. A*, 2014, **2**, 14064–14070.
40 F. Su, C. K. Poh, J. S. Chen, G. Xu, D. Wang, Q. Li, J. Lin and X. W. Lou, *Energy Environ. Sci.*, 2011, **4**, 717–724.
41 Q. Liu and J. Zhang, *Langmuir*, 2013, **29**, 3821–3828.
42 A. Morozan, P. Jegou, B. Jousselme and S. Palacin, *Phys. Chem. Chem. Phys.*, 2011, **13**, 21600–21607.
43 M. Yuasa, A. Yamaguchi, H. Itsuki, K. Tanaka, M. Yamamoto and K. Oyaizu, *Chem. Mater.*, 2005, **17**, 4278–4281.
44 R. Nie, J. Shi, W. Du, W. Ning, Z. Hou and F.-S. Xiao, *J. Mater. Chem. A*, 2013, **1**, 9037–9045.
45 J.-H. Yang, G. Sun, Y. Gao, H. Zhao, P. Tang, J. Tan, A.-H. Lu and D. Ma, *Energy Environ. Sci.*, 2013, **6**, 793–798.
46 S. Li, L. Zhang, J. Kim, M. Pan, Z. Shi and J. Zhang, *Electrochim. Acta*, 2010, **55**, 7346–7353.
47 J. Sun, G. Yu, L. Liu, Z. Li, Q. Kan, Q. Huo and J. Guan, *Catal. Sci. Technol.*, 2014, **4**, 1246–1252.
48 X.-H. Lu, Q.-H. Xia, D. Zhou, S.-Y. Fang, A.-L. Chen and Y.-L. Dong, *Catal. Commun.*, 2009, **11**, 106–109.
49 D. Zhou, B. Tang, X.-H. Lu, X.-L. Wei, K. Li and Q.-H. Xia, *Catal. Commun.*, 2014, **45**, 124–128.